

High-resolution neutron diffraction study of CuNCN: New evidence of structure anomalies at low temperature

Philipp Jacobs,¹ Andreas Houben,¹ Andrei L. Tchougréeff,^{1,2} and Richard Dronskowski^{1,a)}

¹Institute of Inorganic Chemistry, RWTH Aachen University, D-52056 Aachen, Germany

²Lomonosov Moscow State University, Department of Chemistry and Poncelet Laboratory of Mathematics in Interaction with Physics and Informatics, Independent University of Moscow, Moscow Center for Continuous Mathematical Education, Bolshoi Vlasevsky Per. 11, 119002 Moscow, Russia

(Received 9 October 2013; accepted 21 November 2013; published online 12 December 2013)

Copper carbodiimide (CuNCN) is the nitrogen-containing analogue of cupric oxide. Based on high-resolution neutron-diffraction data, CuNCN's lattice parameters are derived as a function of the temperature. In accordance with a recent synchrotron study, a clear trend in the cell parameter a is observed accompanying the changing magnetic behavior. With decreasing temperature, a slowly decreases to a minimum at ~ 100 K after which it rises again. The same trend—albeit more pronounced—is observed for the c lattice parameter at ~ 35 K. The herein presented neutron powder-diffraction data also support the conjectured sequence of transitions from the high-temperature one-dimensional resonating valence-bond (RVB) state to a transient two-dimensional RVB state and eventually, at lowest temperatures, into another two-dimensional RVB state, presumably the ground state. © 2013 AIP Publishing LLC. [<http://dx.doi.org/10.1063/1.4840555>]

I. INTRODUCTION

The magnetic structure of CuNCN has been under investigation ever since its synthesis and structure solution were first reported in 2005 by Liu *et al.*¹ The crystal structure (see Figure 1) was refined from X-ray and neutron-diffraction data^{1,2} resulting in a distorted octahedral coordination of Cu²⁺ by [NCN]²⁻ units due to a first-order Jahn–Teller effect giving rise to four shorter ($d = 2.010(3)$ Å) and two longer ($d = 2.610(4)$ Å) Cu–N bonds. Based on neutron-diffraction data, electrical resistivity, specific heat, and magnetic susceptibility measurements as well as first-principles calculations, CuNCN was first assumed to be a two-dimensional $S = \frac{1}{2}$ frustrated triangular Heisenberg quantum antiferromagnet.² In subsequent publications,^{3–7} a plethora of different magnetic models were proposed including a nonmagnetic ground state,³ an “unconventional” spin glass,⁶ the onset of a magnetic long-range order (LRO) at around 70 K^{4,5} and a resonating valence bond (RVB) state^{6,7} with the latter two being under extensive discussion.

Puzzlingly, CuNCN was described^{4,5} as a uniform spin- $\frac{1}{2}$ chain system with the predominant coupling along c and a very strong antiferromagnetic (AFM) coupling constant ($J \approx 2300$ K).⁵ Additionally, an interchain coupling of approximately $J_1 \approx -500$ K hinted at ferromagnetic (FM) interchain spin alignment along a . This is equivalent to a long-range ordered phase whose presence, however, was previously falsified by spin-polarized neutron measurements.³ Although spin fluctuations might quench the magnetic moment to about $0.4 \mu_B$ ⁵ even that small amount is too large to explain the total absence of magnetic reflections in neutron-diffraction experiments.

Nonetheless, both spin-polarized neutron diffraction and superconducting quantum interference device (SQUID)/ESR measurements of the magnetic susceptibility can be consistently interpreted using an RVB model.^{6,7} One observes⁷ anomalies in the temperature dependence of the a and c lattice parameters around 100 K and an additional anomaly in c at ~ 35 K as detected from synchrotron radiation experiments. This behavior mirrors the transition from a 1D-RVB state at temperatures around 80–100 K to the 2D-RVB state at lower temperatures, and it is also responsible for the switch from the temperature-independent to the activation-like behavior of the magnetic susceptibility. Furthermore, it is in accordance with the absence of reflections in spin-polarized neutron-diffraction experiments.² In order to accommodate the fact that both a and c lattice parameters experience anomalies at lower temperatures, one may⁸ describe the electronic phases of CuNCN by a spatially anisotropic antiferromagnetic Heisenberg Hamiltonian with exchange parameters J_c , J_a , and J_{ac} extending along the c , a , and $a \pm c$ directions in the ac planes, thereby generalizing the Nersesyan–Tsvetlik model.⁹ Supplied with the magnetostriction terms it also qualitatively reproduces the structural effects upon the transition between the different RVB (spin-liquid) phases.⁸

In the following, new high-resolution neutron-diffraction data are presented complementing and extending previous synchrotron experiments,⁷ which are discussed in the light of the magnetic RVB model proposed so far.

II. EXPERIMENT

CuNCN was prepared according to Liu *et al.*¹ High-resolution neutron powder-diffraction data were collected at the Spallation Neutron Source (SNS, Oak Ridge National Laboratory) by means of the POWGEN¹⁰ diffractometer

^{a)}E-mail: drons@HAL9000.ac.rwth-aachen.de. Tel.: +49 (0) 241 80 93642. Fax: +49 (0) 241 80 92642.

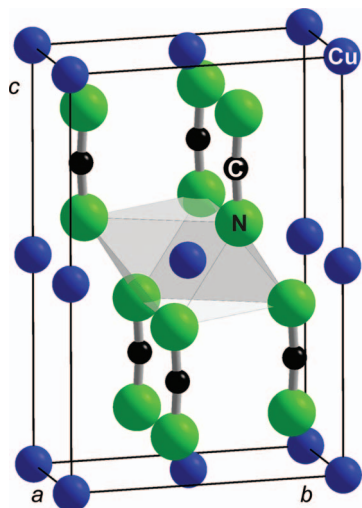


FIG. 1. Crystal structure of CuNCN with copper as blue spheres, carbon as black spheres, and nitrogen as green spheres. The strongly elongated 4+2 octahedral coordination of the copper atoms by the NCN^{2-} units is visible.

operating at two different wavelength bands ($\lambda_1 = 1.066 \text{ \AA}$; d -range: $0.2760\text{--}3.0906 \text{ \AA}$ and $\lambda_2 = 2.665 \text{ \AA}$; d -range: $1.1038\text{--}6.1811 \text{ \AA}$) relating to bank 2 and 5, respectively. Two different data sets were recorded. First, those at selected temperatures between 17 and 140 K which will be denoted as “main data.” The measurement time was approximately 7.5 h for bank 2 and 1 h for bank 5. While cooling the sample from 300 to 25 K, additional data sets were recorded in 25 K temperature steps with short idle times to allow for thermal equilibration. Out of these only data in a temperature window of 10 K around the nominal temperature were taken into account. The acquisition time was around 15 min for each data set, and they will be referred to as “sweep data.” The data treatment concentrates on bank 2 since the region of low d -spacings holds more information. Using the main as well as the sweep data, two different approaches were chosen to extract the results. The first is a standard Rietveld refinement of all data sets. Here, special attention has been paid to the consistency among all measured temperatures by ensuring that the same

sequence of refinement steps was carried out for each temperature. All Rietveld refinements were carried out using the FullProf¹¹ program suite using a pseudo-Voigt profile function with back-to-back exponentials according to the formalism by Hodges *et al.*¹² The backgrounds were manually defined and subsequently smoothed by Fourier filtering. Due to heavy peak overlap, which is characteristic for lower time of flights (TOF), the data below $13\,000 \mu\text{s}$ were excluded. The main refinement parameters together with the results for the 17, 35, and 100 K measurements are summarized in Table I. The parameters for the profile function (with back-to-back-exponentials) are mainly given by the instrument resolution file. Only three of the six parameters describing the half-width as a function of the d_{hkl} -value were carefully refined. It is already known from previous experiments⁷ that the sample exhibits micro-strain. Hence, a broadening model in the quartic form was applied for Laue class mmm .

In a second approach, individual peaks were fitted by a pseudo-Voigt type function without back-to-back-exponentials using the Levenberg–Marquardt^{13,14} algorithm implemented in Gnuplot¹⁵ followed by a regression analysis to yield the lattice parameters for each data set. This approach was chosen to investigate possibly undesired effects of the back-to-back-exponentials on the relative trend of the refined d_{hkl} -values.¹⁶ The peaks used for this approach are (200), (040), (008), (110), (114), (021), (117), (131), (130), (113), and (024), respectively. The conversion between d - and TOF-values was done according to the formalism used in FullProf (see FullProf TOF documentation for $\text{PRF} = 10$). Instead of the usual mixing parameter η we used separate half-width parameters H_k and scale values S for the Gaussian and the Lorentzian part,

$$pV(x) = A + L(x, S_L, H_{k,L}, x_0) + G(x, S_G, H_{k,G}, x_0). \quad (1)$$

A standard F -test comparison between this and the usual function (with η) showed that Eq. (1) is a more suitable description. Using the fitted T -dependent d_{hkl} -values the regression analysis yielded the lattice parameters of the

TABLE I. Main parameters used for the Rietveld refinement of CuNCN data sets including results for the 17, 35, and 100 K measurements.

Temperature (K)	17	35	140
Lattice parameters (\AA)	$a = 2.98908(8)$ $b = 6.1420(3)$ $c = 9.4009(4)$	$a = 2.98892(7)$ $b = 6.1421(3)$ $c = 9.4004(3)$	$a = 2.98892(7)$ $b = 6.1573(3)$ $c = 9.4025(3)$
Volume (\AA^3)	172.59(2)	172.58(2)	173.04(2)
Calculated density (g cm^{-3})	3.9859	3.9863	3.9755
Pattern range, TOF (μs)		13 000–63 000	
Excluded region		0–13 000 and 63 000–80 000	
No. of reflections	276	276	276
No. of parameters	27	27	27
Profile function	pseudo-Voigt with back-to-back exponentials ¹²		
Absorption parameter	0.11(1)	0.12(1)	0.12(1)
Zero, epithermal	Not refined (0 according to instrument resolution file)		
Zero, thermal	Not refined (61.4 according to instrument resolution file)		
R_p	0.0473	0.0435	0.0448
R_{Bragg}	0.0342	0.0346	0.0338

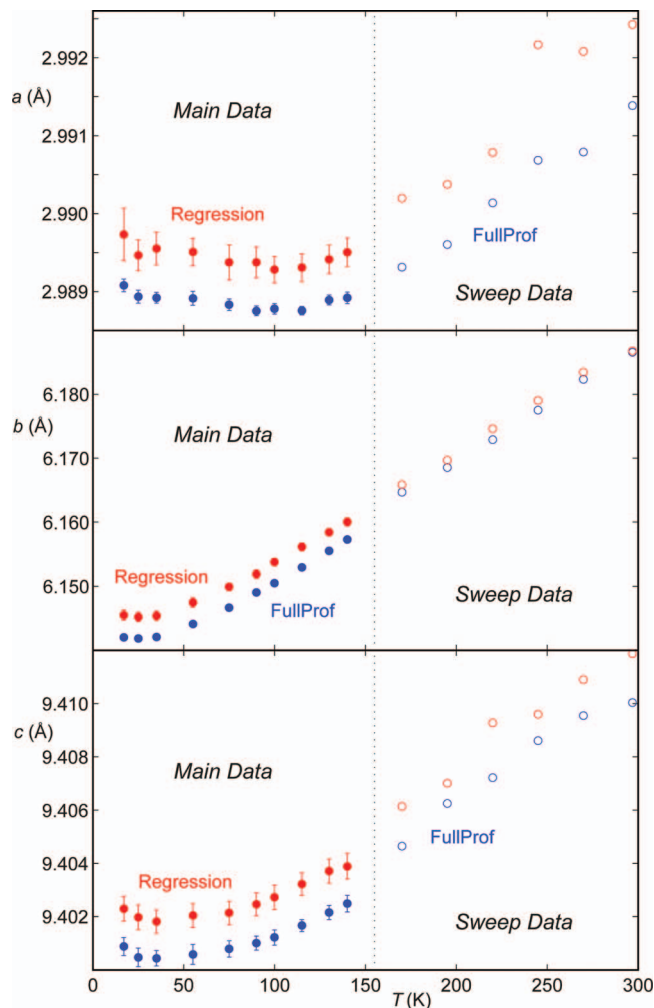


FIG. 2. Comparison of the cell parameters a , b , and c as a function of temperature as derived by the FullProf refinements and the regression calculus. The given errors have been multiplied by the SCOR value (FullProf) and a factor of three (regression), respectively.

orthorhombic crystal system. The statistical errors of the lattice parameters were derived by Gaussian error propagation using the errors of the fitted d_{hkl} values.

III. RESULTS AND DISCUSSION

CuNCN can be considered a corrugated layered structure made up of alternating Cu^{2+} and NCN^{2-} units as depicted in Figure 1. The dianionic NCN^{2-} units run parallel to the c axis and are practically linear ($\angle \text{N-C-N} = 176.4(5)^\circ$). Due to the different bonding types along the three crystallographic axes, a different behavior of the cell parameters with respect to temperature can be expected. The data for a , b , and c as functions of temperature extracted via both methods are shown in Figure 2. Error bars for the sweep data have been omitted for clarity since only the trend is important. It is readily discernible that down to ~ 110 K all lattice parameters show a linear behavior. The slopes within the 100–300 K range are $15(3) \times 10^{-6}$, $177(4) \times 10^{-6}$, and $48(5) \times 10^{-6}$ Å/K for a , b , and c , respectively. Hence, the temperature expansion coefficients are $5(3) \times 10^{-6}$, $29(3) \times 10^{-5}$, and $5(2) \times 10^{-6}$ K $^{-1}$,

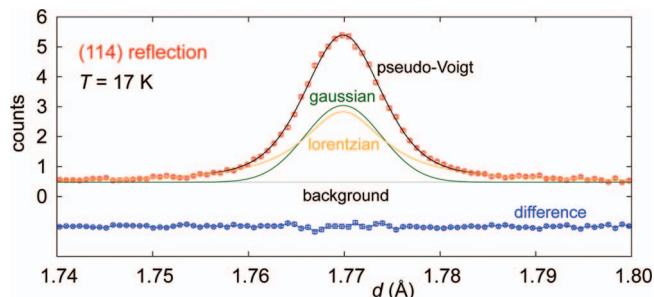


FIG. 3. Results of fitting the neutron data for the (114) reflection at 17 K using a pseudo-Voigt function for the regression calculus.

respectively, with a remarkable similarity for a and c . At temperatures lower than 110 K deviations from this trend start to develop sequentially for a , c , and b at 110–100, 75–80, and below 50 K. The lattice parameters a and c change signs of the slopes of their temperature dependencies at 100 and 35 K, respectively, in good agreement with previous observations.⁷ The lattice parameter b might also show a similar behavior with the lowest value reached at approximately 25 K although the number of data points in the very low temperature region is insufficient to reliably verify or falsify this assumption. Incidentally, any sign change of the slope of the temperature course of b was not observed in the synchrotron data⁷ and the purely two-dimensional version of the theory we use here does not address any characteristics related to b . The extracted values for a , b , and c using FullProf and the regression analysis essentially give the same outcome. For all three lattice parameters, the values obtained via the regression analysis are shifted towards higher values which is explainable by the different profile functions used (FullProf: pseudo-Voigt with back-to-back exponentials; regression: pseudo-Voigt). As has already been laid out by Von Dreele *et al.*¹⁶ incorporating the back-to-back-exponentials leads to a shift of the refined d_{hkl} -value away from the central value to lower d_{hkl} -values. Hence, the asymmetry of the TOF pulse is accommodated. Apart from this shift, we find that the overall trend in cell parameters is almost the same for both approaches. A fit of the (114) reflection at 17 K using the simple pV-function is shown in Figure 3. In contrast to the Rietveld refinement, i.e., a fit including back-to-back exponentials, the d_{hkl} -value is perfectly located at the peak maximum.

Turning now to the interpretation, we first notice that the overall behavior of the lattice parameters as derived from neutron powder diffraction matches the synchrotron data.⁷ We show the lower-temperature segment (< 140 K) in Figure 4 where the temperature course of a and c is presented: a is modeled by a linear approach (experiment: red dots with error bars; linear model: $2.9887 \text{ \AA} - (T - 100 \text{ K}) \times 4.083 \times 10^{-6} \text{ \AA/K}$ as well in red) whereas the temperature course of c (blue dots with error bars) compares with two linear models: one extrapolating the lower-temperature segment of the c behavior in the Pauli-paramagnetic Q1D-RVB phase to the transient 2D-RVB phase (dashed blue line: $9.4003 \text{ \AA} + (T - 35 \text{ K}) \times 20.357 \times 10^{-6} \text{ \AA/K}$) and another 2D-RVB phase (solid blue line: $9.4003 \text{ \AA} - (T - 35 \text{ K}) \times 33.999 \times 10^{-6} \text{ \AA/K}$), valid below 35 K.

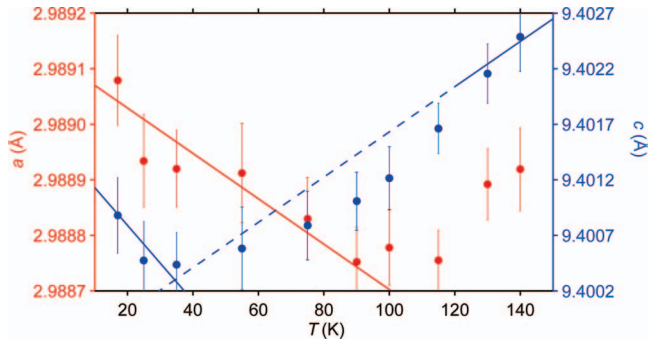


FIG. 4. The temperature dependence of the lattice parameters of CuNCN in the low-temperature region as extracted from neutron diffraction data. The linear models serve to guide the eye.

The deviations of c from being linear in T and the anomalous change of the slope sign of a at the same temperatures is a consequence of an opening pseudogap A for the quasiparticles propagating along a , thereby explaining the transition from the Pauli to the Arrhenius paramagnetic phase. We, therefore, witness a transition from a quasi-one-dimensional RVB (Q1D-RVB) phase⁸ characterized by a gapless quasiparticle spectrum along a , with a bandwidth of $\sqrt{C^2 + 4B^2}$ and a quasiparticle density-of-states which diverges logarithmically at the energy of C (see Figure 5, top), to the transient

two-dimensional RVB (2D-RVB) phase with a quasiparticle bandwidth of $\sqrt{A^2 + C^2 + 4B^2}$ and two pseudogaps at A and C . The latter manifest in the quasiparticle density-of-states (Figure 5, middle) as two logarithmic singularities at the corresponding pseudogap energies. The temperature variation of a and c related to the temperature-dependent pseudogaps A and C ⁸ is given by

$$\begin{pmatrix} \delta a \\ \delta c \end{pmatrix} = \alpha T \begin{pmatrix} a \\ c \end{pmatrix} + \begin{pmatrix} \Lambda_{A,a} \\ \Lambda_{A,c} \end{pmatrix} A^2 + \begin{pmatrix} \Lambda_{C,a} \\ \Lambda_{C,c} \end{pmatrix} C^2. \quad (2)$$

The first term describes the background thermal expansion with the common coefficient α whereas the two terms quadratic in the pseudogap energies describe the effects of the RVB states upon the structure parameters a and c ; the Λ 's are combinations of the magnetic, elastic, and magnetostriction (spin-phonon coupling) and serve as material constants. It may be conjectured⁸ that the temperature dependence of the pseudogap C is the same in the Q1D-RVB and in the transient 2D-RVB phases. Moreover, there C already reaches its limiting value, so that the last term in Eq. (2) does not produce any temperature dependence between 35 and 100 K. With the signs of $\Lambda_{A,a}$ and $\Lambda_{A,c}$ shown to be *opposite*⁸ the structure effect of the transition from the Q1D-RVB to the transient 2D-RVB phase upon a and c must be opposite as well: an increase of a manifests in an extra decrease of c in addition to its background thermal shrinking and that is precisely what we

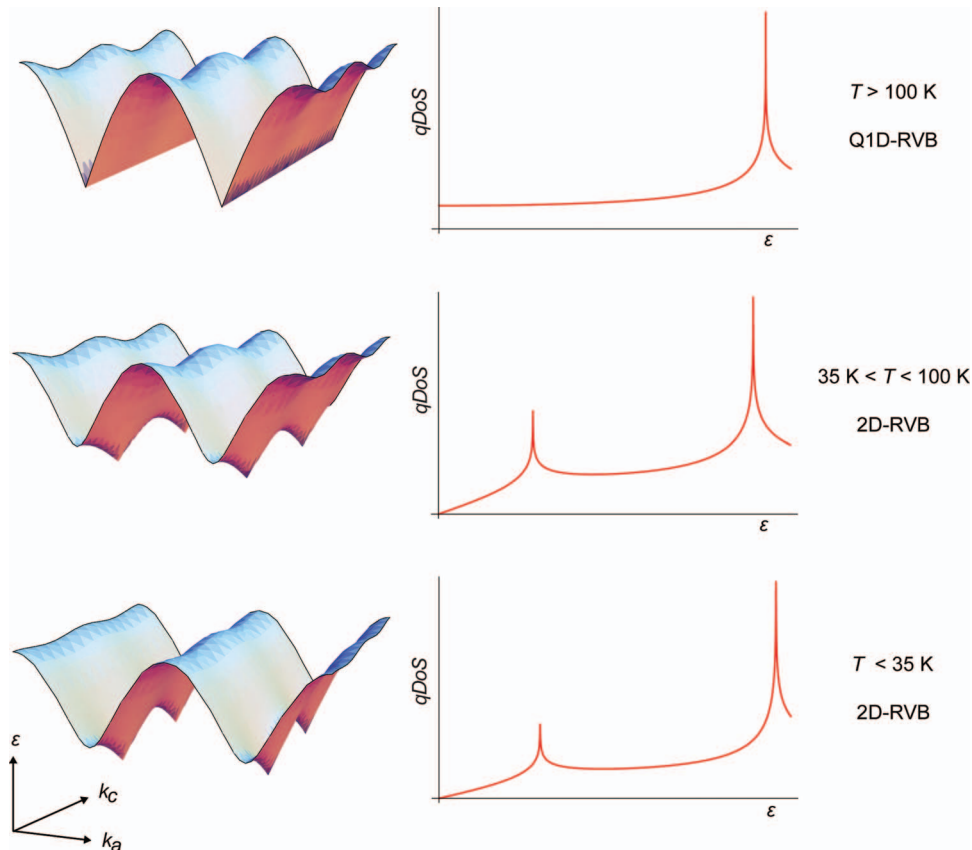


FIG. 5. Characteristics of three RVB phases of CuNCN⁸ in the temperature course of the a and c lattice parameters. The quasiparticle dispersion laws (energy ϵ vs ac planar wave vectors (k_a, k_c)) are shown on the left column for three RVB phases and their quasiparticle density of states (qDoS) on the right. The highest temperature Q1D-RVB phase (top) is gapless along a and yields a finite qDoS at the zero energy. The logarithmic peak occurs at C , the saddles on the dispersion law graph, while the dispersion along c is dominated by the RVB order parameter B . In both 2D-RVB phases (middle and bottom), the dispersion features two pseudogaps A and C showing up as saddles and logarithmic peaks, respectively. The qDoS at lowest energies is linear due to nodal points in the dispersion law.

observe in Figure 4. Although this result qualitatively coincides with the observations made by synchrotron diffraction,⁷ the course of c measured by neutron diffraction now appears much smoother.

The most intriguing events, however, evolve at temperatures lower than 40 K where c changes the sign of its slope,⁷ and the present work confirms this behavior. The sign change of the c vs. T dependency can be attributed to the second RVB phase transition⁸ occurring in the ac crystallographic planes. It must be a transition from the transient 2D-RVB phase which first installs at 100 K or slightly below to the lower-energy 2D-RVB phase which—so far—seems to persist down to zero temperature.¹⁷ The difference between the two 2D-RVB phases is that the B parameter vanishes in the lowest-temperature phase (Figure 5, bottom). Consequently, the free energy of this (ground-state?) phase is lowest as well, which naturally yields the observed sequence of the RVB phase transitions. The quasiparticle spectrum of the latter phase (Figure 5, bottom) very closely resembles the spectrum of the former transient 2D-RVB phase (both have four nodal points and two pseudogaps: A and C in the dispersion laws of the respective quasiparticles) but the quasiparticle densities-of-states slightly differ. The one belonging to the lowest-temperature 2D-RVB phase is concentrated in a narrower energy interval, since its quasiparticle bandwidth is $\sqrt{A^2 + C^2}$ as compared with $\sqrt{A^2 + C^2 + 4B^2}$. Hence, the pseudogap C manifests a temperature dependence in the lowest-temperature 2D-RVB phase; namely, it starts decreasing along with the temperature decrease from its limiting value in the Q1D-RVB and the transient 2D-RVB phases. The pseudogap A , by contrast, can be assumed to reach its limiting value when the second phase transition occurs at ~ 40 K. The slope of the temperature dependence of c changes its sign as compared to the transient 2D-RVB and Q1D-RVB phases because the sign of $\Lambda_{C,c}$ is negative.⁸ Thus, the transition between the two 2D-RVB phases is now confirmed by neutron diffraction. Indeed, a change of slope in the a vs. T dependency was already predicted to signal the 2D-RVB phase change.⁸ This is depicted in Figure 4—at least strong irregularities of the course of a below 35 K, but clearly the increase of the negative slope of a vs. T by its absolute value, which implies the negative sign of $\Lambda_{C,a}$. Unfortunately, our current knowledge of the magnitude of the magnetic, elastic, and magnetostriction parameters is still insufficient to make more quantitative comparisons. The same applies to the exact form of the temperature dependence of the pseudogaps A and C which also needs a more detailed study.

IV. CONCLUSION

High-resolution neutron powder-diffraction data of CuNCN were collected at the POWGEN instrument. The analysis using two approaches confirms the anomalous trend of the a and c lattice parameters within the orthorhombic crys-

tal system. The a lattice parameter reaches its minimum value at around 100 K and increases at lower temperatures while c exhibits the same behavior with its minimum value at around 35 K. This is in good agreement with previous data based on synchrotron measurements. A similar behavior of the b parameter with a minimum at ~ 25 K may be suspected, but is not firmly established. The current magnetic model does not allow for any predictions for b as the model only depends on interactions along a and c . A confirmation of anomalies along b might, therefore, indicate that further interactions need to be considered to describe the fascinating physics of CuNCN. Otherwise the observed behavior confirms^{6–8} a sequence of transitions between the various spin-liquid (RVB) phases of CuNCN which occur upon decreasing the temperature. This unites the results of polarized neutron, magnetic, and structural measurements into a single picture.

ACKNOWLEDGMENTS

The authors gratefully acknowledge the financial support provided by JCNS to perform the neutron scattering measurements at the Spallation Neutron Source (SNS), Oak Ridge, USA. Part of the Research conducted at SNS was sponsored by the Scientific User Facilities Division, Office of Basic Energy Sciences, U.S. Department of Energy. The authors want to thank Olivier Gourdon and Ashfia Huq at the SNS for their kind help during the measurements. The authors also thank Xiaojuan Tang for preparing the CuNCN samples.

- ¹X. Liu, M. A. Wankau, H. Lueken, and R. Dronskowski, *Z. Naturforsch.* **60b**, 593 (2005).
- ²X. Liu, R. Dronskowski, R. Kremer, M. Ahrens, C. Lee, and M.-H. Whangbo, *J. Phys. Chem. C* **112**, 11013 (2008).
- ³H. Xiang, X. Liu, and R. Dronskowski, *J. Phys. Chem. C* **113**, 18891 (2009).
- ⁴A. A. Tsirlin and H. Rosner, *Phys. Rev. B* **81**, 024424 (2010).
- ⁵A. A. Tsirlin, A. Maisuradze, J. Sichelschmidt, W. Schnelle, P. Höhn, R. Zinke, J. Richter, and H. Rosner, *Phys. Rev. B* **85**, 224431 (2012).
- ⁶A. Zorko, P. Jeglič, A. Potočnik, D. Arčon, A. Balčytis, Z. Jagličić, X. Liu, A. L. Tchougréeff, and R. Dronskowski, *Phys. Rev. Lett.* **107**, 047208 (2011).
- ⁷A. L. Tchougréeff, X. Liu, P. Müller, W. van Beek, U. Ruschewitz, and R. Dronskowski, *J. Phys. Chem. Lett.* **3**, 3360 (2012).
- ⁸A. L. Tchougréeff and R. Dronskowski, *J. Phys.: Condens. Matter* **25**, 435602 (2013).
- ⁹A. A. Nersisyan and A. M. Tselik, *Phys. Rev. B* **67**, 024422 (2003).
- ¹⁰A. Huq, J. P. Hodges, O. Gourdon, and L. Heroux, *Z. Kristallogr. Proc.* **1**, 127 (2011).
- ¹¹J. Rodríguez-Carvajal FULLPROF2000, version 3.2, Laboratoire Léon Brillouin, Gif sur-Yvette Cedex, France, 1997.
- ¹²See <http://neutrons.ornl.gov/powgen/run-cycles/2012-b/Powgen-profile-function.pdf> for POWGEN instrument homepage.
- ¹³D. W. Marquardt, *J. Soc. Ind. Appl. Math.* **11**, 431 (1963).
- ¹⁴K. Levenberg, *Q. Appl. Math.* **2**, 164 (1944).
- ¹⁵See <http://www.gnuplot.info/> for Gnuplot homepage.
- ¹⁶R. B. Von Dreele, J. D. Jorgensen, and C. G. Windsor, *J. Appl. Crystallogr.* **15**, 581 (1982).
- ¹⁷A. L. Tchougréeff and R. Dronskowski, *Low Temp. Phys. (Fiz. Nizk. Temp.)* **40**, 92 (2014).